Scaling structure of tracer dispersion fronts in porous media

Aleksandar Birovljev, Knut Jørgen Måløy, Jens Feder, and Torstein Jøssang
Department of Physics, University of Oslo, Box 1048 Blindern, N-0316 Oslo 3, Norway
(Received 7 February 1994)

Experiments on the miscible displacement of a clear fluid by a dyed fluid of the same viscosity and density in a rectangular quasi-two-dimensional porous medium are presented. Equiconcentration dispersion fronts were identified using computer image processing. The fronts taken at three different concentrations are fractal curves with approximately the same box fractal dimension $D \simeq 1.45$. In an alternative analysis the fronts were reduced to single valued functions and the dynamic scaling behavior investigated using a self-affine scaling formalism. The Hurst exponent $H = 0.55$ and the dynamic exponent $\beta = 0.5$, found by collapsing height difference correlation function data, are consistent with the results obtained through other analysis methods. The average concentration profile across the dispersion front was found to follow the classical solution of the diffusion-convection equation. The dependence of the width of the equiconcentration dispersion front σ on time yields dispersion coefficients D_σ over one order of magnitude less than the longitudinal dispersion coefficient $D_{\|}$.

PACS number(s): 47.55.Mh, 47.55.Kf, 05.40.+j

I. INTRODUCTION

The process of tracer dispersion in porous media is a complex interplay between molecular diffusion and convective mixing. Applications range from petroleum and chemical engineering to hydrology and chemical or nuclear waste storage.

The classical description of Gaussian (normal) dispersion in a disordered, multiply-connected and homogeneous medium is by the macroscopic convection-diffusion equation [1–4]:

$$\frac{\partial C}{\partial t} + U\frac{\partial C}{\partial x} = D_{\|}\frac{\partial^2 C}{\partial x^2} + D_\perp \nabla_\perp{}^2 C. \qquad (1)$$

Here $C(\mathbf{x}, t)$ is the tracer concentration as a function of position $\mathbf{x}$ and time t. The longitudinal $D_{\|}$ and transversal dispersion coefficient $D_\perp$, as discussed extensively by Bear [4], depend in general on the imposed hydrodynamic (average) flow velocity $\mathbf{U}$. These two coefficients are of major interest in most dispersion studies and in particular their dependence on the velocity U. The dimensionless *Péclet* number $\mathrm{Pe} = Ua/D_m$ measures the ratio between typical diffusion time and convection time over a length scale a. Here a is the typical pore size and D_m is the diffusion constant of tracers in the fluid.

At the microscopic level the flow through a porous medium depends on the detailed structure and geometry of the pore space. The presence of the solid part of the medium forces the streamlines to meander through the pore volume giving rise to a distribution of path lengths. The streamlines through one pore may separate into different pores and also meet again in a later pore. The velocity along a single streamline also fluctuates being slow through narrow pores and in stagnant regions, and faster than the average flow in wide pores oriented parallel to the average flow. The tracer particles that are carried by the streamlines from one pore to another appear to be effectively performing random walks through the medium.

In the limit of very low Pe the molecular diffusion is the dominant mechanism of tracer transport and $D_{\|} = D_\perp = D_m/\alpha$ where α ($\alpha > 1$) is the tortuosity constant that accounts for geometrical restrictions of the porous medium.

For large Péclet numbers mechanical mixing dominates and dispersion in this regime is often called geometrical or mechanical dispersion. Taking mean position of the dispersion front to be the reference point (origin) moving with constant, average velocity of the flow, the movement of the tracer particles may be understood as a one-dimensional random walk process. The effective diffusion constant is calculated from the Einstein relation: $D_{\|} = \frac{1}{2}a^2/\tau$, where the average time between "steps" of length a is $\tau \sim a/U$. Therefore [1] $D_{\|} \sim Ua$, i.e., the longitudinal dispersion is proportional to the flow velocity U for $\mathrm{Pe} \gg 1$. For media with significant presence of stagnation zones (regions of very low flow velocity) the expression for the dispersion coefficient is modified by logarithmic terms $D_{\|} \sim Ua\ln(U\ell/D_m)$, where ℓ is a length scale related to the transport out of stagnant regions [1,3,5].

In the regime of intermediate Péclet numbers, the interplay between the transverse diffusive mixing and convection leads to *Taylor dispersion* [6] with the longitudinal dispersion coefficient given by $D_{\|} = D_m + a^2U^2/48D_m$. Taylor derived and measured this dependence for the capillaries of radius a. Taylor dispersion dominates if the transverse mixing is large enough, i.e., if the time needed for diffusion across the capillary a^2/D_m is short enough compared with the convective time a/U.

The pioneering works by Taylor [6] and Saffman [1] do not treat the influence of the disorder of the porous medium, such as the pore size distribution, on the dis-

 ©1994 The American Physical Society

persion. It is not until recently that the new simulations and theoretical methods [5,7] have been used to investigate how randomness affects the hydrodynamic dispersion. The influence of the disorder effects has been explored experimentally by Bacri *et al.* [8] by performing *in situ* measurements using an acoustic technique. For flow rates in the intermediate regime between the pure diffusion regime and the geometrical dispersion regime they found a dispersion coefficient that was strongly dependent on the randomness of the porous medium consistent with the results of Arcangelis *et al.* [7].

Few experiments on dispersion focused on the microscopic structure of the dispersion fronts [5,9]. Recent work by Måløy et al. [9] at high Péclet numbers shows that the concentration contours at a single concentration level $C/C_0 = 0.5$ are fractal with a fractal dimension $D \simeq 1.42$. These experiments were done in a radial geometry where the mean velocity of the flow decreases with time. So far there is no theoretical explanation of the fractal nature of these dispersion fronts.

In this paper we visualize and analyze dispersion front in a quasi-two-dimensional porous strip, different from the radial geometry used earlier in that the mean velocity of the flow is constant at every cross section of the strip. We find that the dispersion front on the average is accurately described by Eq. (1) at high Péclet numbers where convection dominates. Analysis of the *equiconcentration dispersion fronts* (EDF), consisting of points (pixels) of a certain local concentration of tracer confirms the same fractal dimension as found in the radial geometry [9]. This analysis, done at three different concentration levels, gives the same fractal dimension for all the concentrations indicating no multifractal behavior. Self-affine scaling analysis of the *reduced EDF's* yields the same values for the Hurst exponent and the dynamic exponent β for all concentrations considered. We also study the time dependence of the equiconcentration front width and find an effective equiconcentration dispersion constant of one order of magnitude less than the longitudinal dispersion constant. Comparisons to other types of rough surfaces are mentioned and discussed.

II. EXPERIMENTS AND ANALYSIS TECHNIQUE

The experiments were performed using transparent quasi-two-dimensional porous model consisting of a monolayer of 1 mm glass beads. The homogeneous porous medium was produced by throwing beads at random on the sticky surface of the contact paper sheet until no place for additional beads was left [10,11]. The monolayer of beads is covered with another sheet of contact paper. The boundaries of the medium were provided using 1 mm silicone rubber stripes. The model had dimensions 400×200 mm, porosity $\phi \simeq 0.7$, and was supported between two 25 mm polymethylmethacrylate plates. The contact paper sheets were forced into contact with the beads by a transparent PVC air pillow inflated between a supporting plate and one of the sheets. The displacement process was visualized by illuminating the model from below and the photographs were taken from above.

The dispersion experiments were done by injecting a glycerol with 13% water mixture dyed with black Nigrosine dye into a medium saturated with the same fluid without the dye. The fluid properties were viscosity: $\mu = 118 \pm 0.4$ cP, density: $\rho = 1.21 \pm 0.03$ g/cm^3, temperature: T = 25 °C. The diffusion constant of the Nigrosine particles in the fluid was $D_m \simeq 1 \times 10^{-8}$ cm^2/s. The injection was conducted at rate $Q = 0.028$ cm^3/s from a "line" (high permeability channel at the shorter edge of the rectangular model). The Péclet number in a typical experiment was 4×10^4.

The porous model was divided into two sections separated by a thin barrier (straight metal wire) which was placed perpendicularly to the direction of the flow. The smaller section of the medium was saturated with dyed fluid and the larger one with clear fluid. Experiment was started by activating an injection pump which was connected to the smaller section of the medium and simultaneously removing the barrier between dyed and clear sections. This technique generated a sharp, linear initial interface. About 20 photographs were taken during one experiment.

The resulting dispersion of the Nigrosine dye was photographed and the negatives digitized with a resolution of up to 2000×2000 pixels using a Nikon LS-3500 film scanner connected to an Apollo computer workstation. In the digitizing procedure we selected a logarithmic response curve so that the resulting grey levels (0–255) were roughly proportional to the concentration of Nigrosine in the volume imaged onto a pixel. In Fig. 1 a calibration curve relating the grey levels to the concentration is given. As can be seen from this plot, the linearity in the intermediate concentration range is good, but some deviations at extreme concentrations are present.

A high resolution digitized photograph of a fully developed dispersion front is shown in Fig. 2 (a). The figure illustrates strong fluctuations of the dispersion front caused by geometrical (convective) dispersion, which gen-

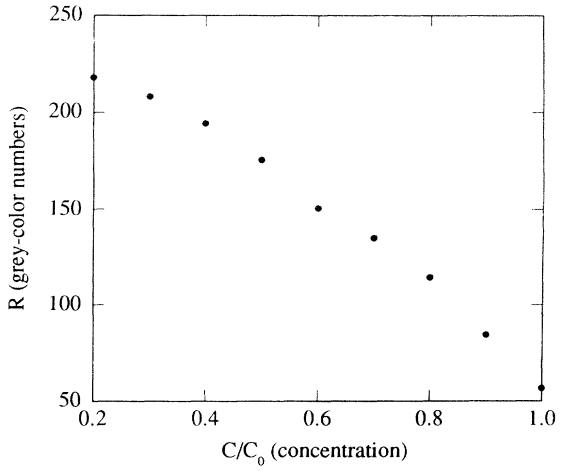

FIG. 1. Calibration of the digitizing equipment: grey levels as a function of Nigrosine concentration.

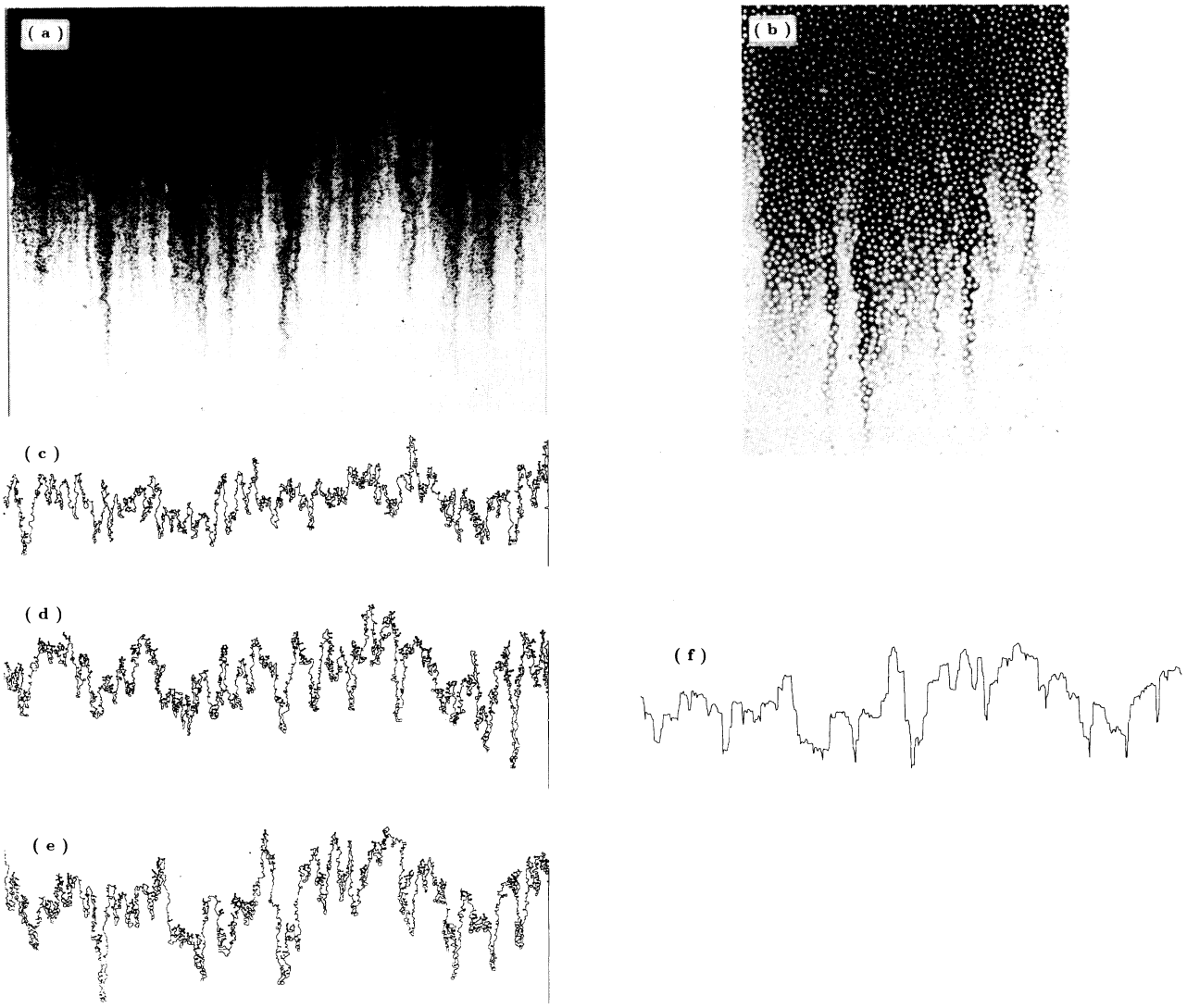

FIG. 2. (a) Digitized photograph of the dispersion front. The experiment was conducted at Péclet number Pe $\simeq 4 \times 10^4$. The size of the image is 1000 × 700 pixels. (b) Close-up photograph of the dispersion front showing concentration variation from the sub pore size scale up to the tens of pore sizes. White dots in the photo are glass beads. (c)–(e) Development of an equiconcentration dispersion front at relative concentration $C/C_0 = 0.4$. The fronts were taken at times: 135 s (c), 254 s (d), and 400 s (e). The front at time t=400 s was reduced to a single value function by replacing parts of the curve within overhangs by straight line segments in x direction (d).

erates large scale concentration "spikes" in the longitudinal x direction due to the flow velocity fluctuations and the streamline path length fluctuations. Effectively, the structure results because the transverse mixing (dispersion) controlled by coupling between diffusion and convective transport is not sufficient to average out large longitudinal fluctuations caused in the velocity field.

A close-up photograph of the dispersion front depicted in Fig. 2 (b) shows concentration fluctuations from below the pore size scale up to the several tens of pore sizes. The dark "fingers" of the dyed liquid penetrating clear liquid trace the fastest streamlines and are the consequence of the separation of streamlines as they flow around the beads. This gives rise to large concentration gradients. Larger separations between the fingers (low concentration regions) appear behind regions of slightly lower permeability or stagnation zones. On the pore level stagnation points are the points mostly shielded from the flow (exactly behind each bead). The fingers and the separations among them appear to have widths ranging from below pore size up to several pore sizes. These initially large concentration gradients are smeared out at a later time due to diffusion and the coupling between diffusive and convective motion of the tracer particles.

The digitized images of the dispersion front containing 256 different grey levels were converted into black-white images by the following procedure. All the pixels in the image with grey levels below a chosen level (concentration) were assigned value zero and the others value one. Equiconcentration dispersion fronts were identified

in such black-white images as coast lines of connected pixels. The search for this coast line was done starting from the low concentration region. Details of a similar analysis are found in Ref. [11]. Three stages in the development of an EDF at relative concentration $C/C_0 = 0.3$ during one experiment is shown in Figs. 2(c)–2(e) .

The spatial resolution used in the digitizing procedure corresponds to 0.2 mm per pixel, meaning that we detect concentration change at a subpore-size scale. Such resolution, combined with the spherical geometry and the light scattering by the beads, introduce some imprecision when identifying EDF's. This may be seen in Figs. 2(a)–2(c) in the form of small circles due to the presence of the beads. The circles are, however, evenly distributed along the front. Although the circles may affect absolute value of the EDF width σ they are unlikely to cause problems for the scaling of σ with time or the study of the front roughness at a scale larger than the pore size.

III. RESULTS

Concentration profiles of the dispersion front plotted in Fig. 3 were obtained by summing up grey levels of the digitized dispersion images in the direction y perpendicular to the flow . A good approximate solution of Eq. (1) with the initial and boundary conditions used in the experiment is given by

$$C(x,t) = \frac{1}{2}\{1 - \mathrm{erf}[(x - X_0)/\lambda]\}. \quad (2)$$

Here $\mathrm{erf}(x)$ is the error function, $X_0 = Ut$ is the position of the front, and $\lambda = 2\sqrt{D_{\|}t}$ is the *average concentration profile width.* In Fig. 3 curves of the form given by Eq. (2) are fitted to the experimental concentration profiles of a typical dispersion experiment. The figure shows that Eq. (2) (full curves) approximates the observed concentration profile well. At high concentration region we observe stronger noise compared to the low concentration region. This is partly due to a decreased sensitivity at low concentrations since the calibration curve in Fig. 1 enters a saturation regime.

Another effect resulting in larger spread of data at high concentrations is due to the presence of the glass beads. Each point in Fig. 3 is a grey level average across the porous model, meaning that we also sum over grey levels that belong to the beads which transmit light and therefore have a very low grey level. This means that the sum of grey levels will depend on the number of beads in a particular cross section. This dependence will be particularly strong in the high Nigrosine concentration range due to the strong contrast in grey level values of the pixels belonging to the beads and those belonging to the liquid.

The concentration profile width λ is obtained as a fitted parameter of error curves in Fig. 3. The longitudinal dispersion coefficient is then estimated as a slope of λ^2 vs t plot as shown in Fig. 4. The least square fit in this plot yields $D_{\|} \simeq 0.094 \pm 0.006$ cm^2/s. Here, the error reflects the statistical uncertainty for the given data set.

The equiconcentration front width σ is defined as the standard deviation of the distribution obtained by counting the number of front sites as a function of position x. The distribution is centered at the mean position of the front. Note that σ is a single concentration front-width as compared to λ which describes the typical width of the average concentration profile consisting of the whole spectrum of concentrations.

The structure of EDF was studied in terms of the box dimension of the perimeters. The EDF's were identified from 6 digitized images taken during one experiment using three different values of the grey levels (local concentrations). The number N of square boxes of side δ needed to cover the front scales as

$$N(\delta) = N_0 \sigma^{-D} f(\delta/\sigma), \quad (3)$$

where D is the fractal dimension of the front, $f(x)$ is a function depending only on the combination δ/σ, and N_0 is the number of boxes of size $\delta = a$. Fitting $\log_{10}(N(\delta)\sigma^D/N_0)$ to the straight line $D\log_{10}(\delta/\sigma) + A$ where D and A are the only two free parameters gave us

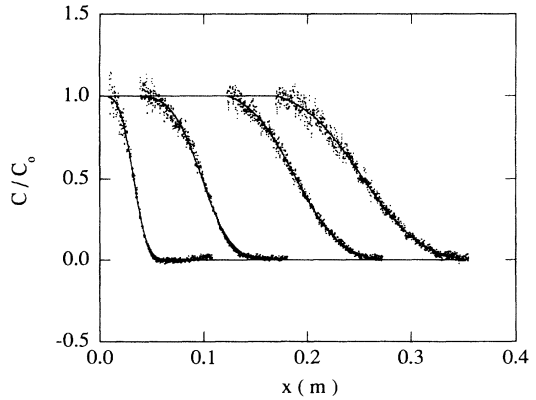

FIG. 3. The concentration profile as a function of x at different times. The full curves are the least square fit to the experimental data. The effective width of such a front λ is obtained directly as a fitting parameter. Péclet number is Pe $\simeq 4 \times 10^4$.

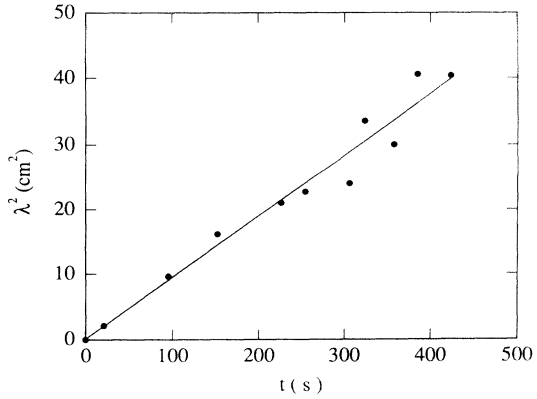

FIG. 4. The effective width, λ squared versus t gives a straight line. The slope of this line is dispersion coefficient $D_{\|} \simeq 0.094 \pm 0.006$ cm^2/s. Péclet number is Pe $\simeq 4 \times 10^4$.

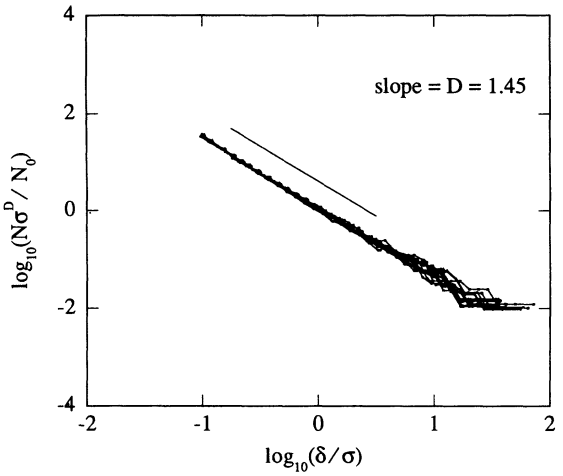

FIG. 5. Data collapse of the box-counting data for 16 equiconcentration dispersion fronts. The box dimension was found to be $D = 1.45 \pm 0.04$.

the best scaling data collapse in Fig. 5. The figure shows collapsed data of 16 EDF's taken at three different concentrations, $C/C_0 = 0.3$, 0.4, and 0.8. The fitting procedure yields the same fractal dimension $D = 1.45 \pm 0.04$ for all fronts. Crossover to Euclidean, one-dimensional objects is expected at the rescaled box size $\delta/\sigma \simeq 3$. Note that, although the EDF's are fractal, the concentration profiles which are the average of all concentrations are well described by Eq. (2).

Treating EDF as a self-affine fractal object an alternative analysis has been conducted. EDF's were analyzed using the second order height difference correlation function:

$$C_2(r) = \langle |h(y) - h(y+r)|^2 \rangle^{1/2}, \tag{4}$$

where y is the direction perpendicular to the flow and $h(y)$ is the height of the front above position y on a reference line. For this analysis to work EDF's, as those depicted in Figs. 2(c)–2(e), had to be reduced to a single valued function. This has been done by replacing parts of the front cut by overhangs in the original fronts by straight line segments. An example of the resulting *reduced* EDF is shown in Fig. 2 (f). A short review of the self-affine scaling formalism for rough surfaces [12–14], adequate for our problem, is presented below.

For statistically self-affine fractals this function scales with r as $C_2 \sim r^H$, where H is the Hurst exponent, a measure of surface roughness and related to the fractal dimension through

$$H = d - D \tag{5}$$

in d dimensional space. The self-affine scaling range is bounded in space by two correlation lengths $\xi_\perp$ (front width) in x direction and $\xi_\parallel$ in y direction. The height difference correlation function in general scales as

$$C_2(r) = \xi_\perp f(r/\xi_\parallel). \tag{6}$$

Here $f(y)$ is the crossover function which is constant for $r \gg \xi_\parallel$ and proportional to y^H for $r \ll \xi_\parallel$.

Rough surfaces exhibit often dynamic scaling:

$$\xi_\perp \sim t^\beta, \tag{7}$$

$$\xi_\parallel \sim t^{\beta/H}, \tag{8}$$

with a dynamic exponent β. In a finite system the scaling in Eqs. (7) and (8) is valid as long as $\xi_\parallel$ is less than the size of the system. Inserting Eqs. (7) and (8) into Eq. (6) the following combined scaling form is obtained:

$$C_2(r) = t^\beta f\left(\frac{r}{t^{\beta/H}}\right). \tag{9}$$

In Fig. 6 a data collapse for reduced EDF's is attempted by plotting the crossover function f after Eq. (9). The data for $C/C_0 = 0.4$ and $C/C_0 = 0.3$ are shifted by 0.8 and 1.6, respectively, in the $+y$ direction for better view of the data points. The parameters β and H were varied until the best collapse with $\beta = 0.5$ and $H = 0.55$ for all three concentrations was obtained in Fig. 6. Note that the value for H is in excellent agreement with Eq. (5) using value for D found by box-counting procedure. The value for β characterizing temporal behavior of the reduced EDF widths agrees with the corresponding expo-

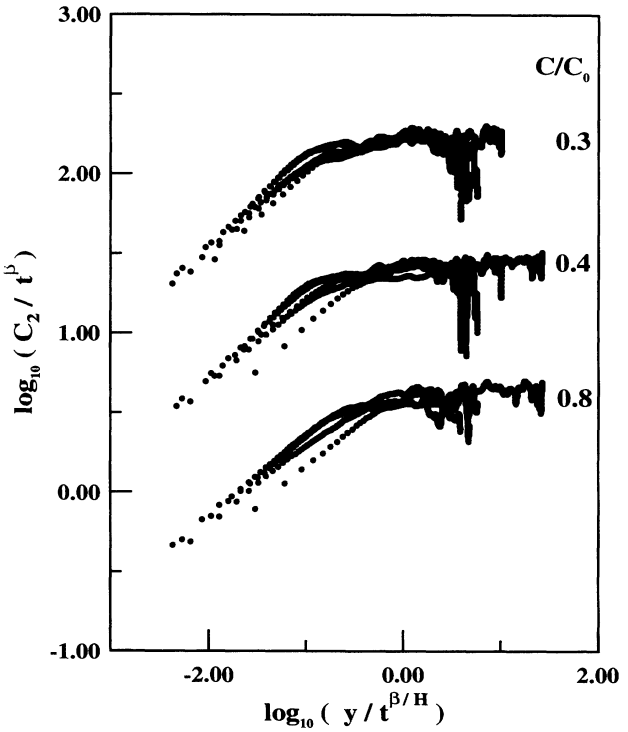

FIG. 6. Height difference correlation functions $C_2(y)$ for three different relative concentrations are attempted collapsed. Exponents β and H were varied as free parameters until the shown best collapse of the data with $\beta = 0.5$ and $H = 0.55$ was found. See discussion in the text. The data for $C/C_0 = 0.4$ and $C/C_0 = 0.3$ are shifted by 0.8 and 1.6, respectively, in the $+y$ direction for better view of the data points.

nent used for scaling of the average concentration profile width λ (see Fig. 4).

We further investigated the dependence of the equiconcentration front width σ on time for the three concentrations. Such a plot is given in Fig. 7 . There appears to be no significant difference in width σ for different concentrations. A straight line has been fitted to the data for each concentration. Note that the straight line is not required to pass through the point (0,0) due to uncertainty of the initial front widths. The average slope is $D_\sigma \simeq 0.0036$. This value is over one order of magnitude smaller than $D_{||} \simeq 0.09$.

IV. DISCUSSION

The concentration profiles of the dispersion front in a quasi-two-dimensional, rectangular porous medium have been measured. The average concentration along the channel is described quite well by the solution of the convection-diffusion Eq. (1) in a channel which is given in Eq. (2). The value of longitudinal dispersion coefficient for one velocity has been measured to be $D_{||} \simeq 0.094 \pm 0.006$ cm^2/s.

Measuring the time development of the width σ of the EDF's for three different concentrations ($C/C_0 = 0.3$, 0.4, and 0.8) enabled determination of the equiconcentration dispersion coefficient D_σ of each of the three concentrations. It appears that $D_\sigma \simeq 0.0036$ has similar value within the error of the measurement for the three concentrations considered, and is roughly an order of magnitude less than the average dispersion coefficient $D_{||}$. This perhaps surprising result appears to be a consequence of different EDF's moving with different average speeds, effectively drifting apart. Both width of the average concentration profile λ and the EDF width σ though depend on time as a square root.

The detailed structure of EDF's in a quasi-two-dimensional porous medium is found to be fractal, confirming the finding of Måløy *et al.* [9] for radial geometry and for only one concentration $C/C_0 = 0.5$. All fronts were found to have the box dimension $D = 1.45 \pm 0.04$.

Compared to percolation-perimeters related structures [15] EDF represent a different class of problems. Diffusion front of Sapoval *et al.* [16] or the gravity stabilized invasion percolation front [17] are examples of a crossover from self-similar behavior at length scale less than front width to linear behavior at larger length scale. With EDF's the dynamic scaling of the correlation length $\xi_{||}$ is different from that of $\xi_\perp$ on all length scales [Eqs. (7) and (8)]. The scaling structure of EDF is therefore always self-affine.

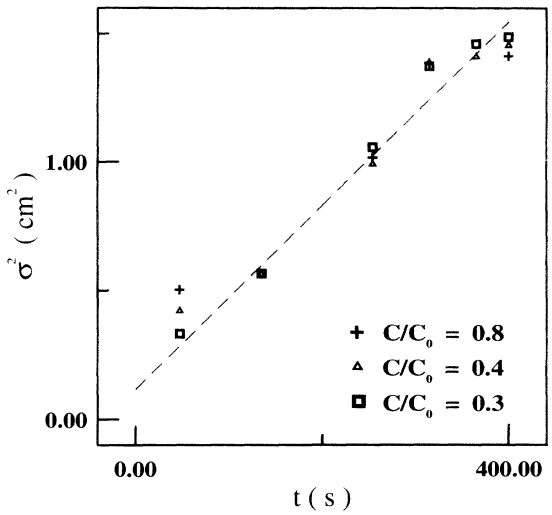

FIG. 7. Dependence of equiconcentration front widths σ on time. Three different concentrations were used: $C/C_0 = 0.3$ (△) , 0.4 (○), and 0.8 (□). The average slope for the three concentrations obtained by the least squares fit to the data yields $D_\sigma \simeq 0.0036$.

In the limit Pe $\to 0$ a smooth, linear diffusion front is expected. As noted in Ref. [15] the fractal dimensions of the external perimeter of the percolation cluster is 4/3 while the percolation hull has $D = 7/4$. The measured box dimension for EDF, $D \simeq 1.45$, although closer to 4/3 is somewhere in between.

Reduced EDF's were analyzed as self-affine fractals. The Hurst exponent $H = 0.55$ and the dynamic exponent $\beta = 0.5$ found by collapsing height difference correlation function data are consistent with the results obtained through other analysis methods. The found value of H appears to be not too far from 0.5 which is characteristic of independent Gaussian processes [18].

ACKNOWLEDGMENTS

We thank Paul Meakin for useful suggestions. We gratefully acknowledge support by VISTA, a research cooperation between the Norwegian Academy of Science and Letters and Den norske stats oljeselskap a.s. (STATOIL) and by NAVF the Norwegian Research Council for Science and the Humanities.

[1] P. G. Saffman, J. Fluid Mech. **6**, 321 (1959); **7**, 194 (1960).

[2] D. F. Koch and J. F. Brady, J. Fluid Mech. **154**, 399 (1985).

[3] C. Baudet, E. Charlaix, E. Clement, E. Guyon, F. P. Hulin, and C. Leroy, in *Scaling Phenomena In Disordered Systems,* edited by R. Pynn and T. Riste (Plenum, New York, 1985), p. 399.

[4] J. Bear, *Dynamics of Fluids in Porous Media* (American Elsevier, New York, 1972); A. E Scheidegger, *The Physics of Flow Through Porous Media* (University of Toronto Press, Toronto, 1974); A. L. Dullien, *Fluid Transport and Pore Structure* (Academic Press, New York, 1979).

[5] E. Charlaix, J. P. Hulin, and T. J. Plona, C. R. Acad.

Sci. Ser. 2 **303**, 1413 (1986); E. Charlaix, J. P. Hulin, and T. J. Plona, Phys. Fluids **30**, 1690 (1987).
[6] G. I. Taylor, Proc. R. Soc. London Ser. A **219**, 186 (1953).
[7] L. de Arcangelis, J. Koplik, S. Redner, and D. Wilkinson, Phys. Rev. Lett. **57**, 996 (1986); S. Roux, C. Mitescu, E. Charlaix, and C. Baudet, J. Phys. A **19**, L687 (1986).
[8] J. C. Bacri, N. Rakotomalala, and D. Salin, Phys. Rev. Lett. **58**, 2035 (1987).
[9] K. J. Måløy, J. Feder, F. Boger, and T. Jøssang, Phys. Rev. Lett. **61**, 2925 (1988).
[10] K. J. Måløy, F. Boger, J. Feder, T. Jøssang, and P. Meakin, Phys. Rev. A **36**, 318 (1987).
[11] A. Birovljev, Master's thesis, University of Oslo, 1990.
[12] T. Vicsek, *Fractal Growth Phenomena* (World Scientific, Singapore, 1992).
[13] P. Meakin, Phys. Rep. **235**, 189 (1993).
[14] T. Jøssang and J. Feder, Phys. Scr. **T44**, 9 (1992).
[15] T. Grossman and A. Aharony. J. Phys. A **19**, L745 (1986); **20**, L1193 (1987).
[16] B. Sapoval, M. Rosso, and J. F. Gouyet, J. Phys. Lett. **46**, L149 (1985).
[17] A. Birovljev, L. Furuberg, J. Feder, T. Jøssang, K. J. Måløy, and A. Aharony, Phys. Rev. Lett. **67**, 584 (1991).
[18] J. Feder, *Fractals* (Plenum, New York, 1988).

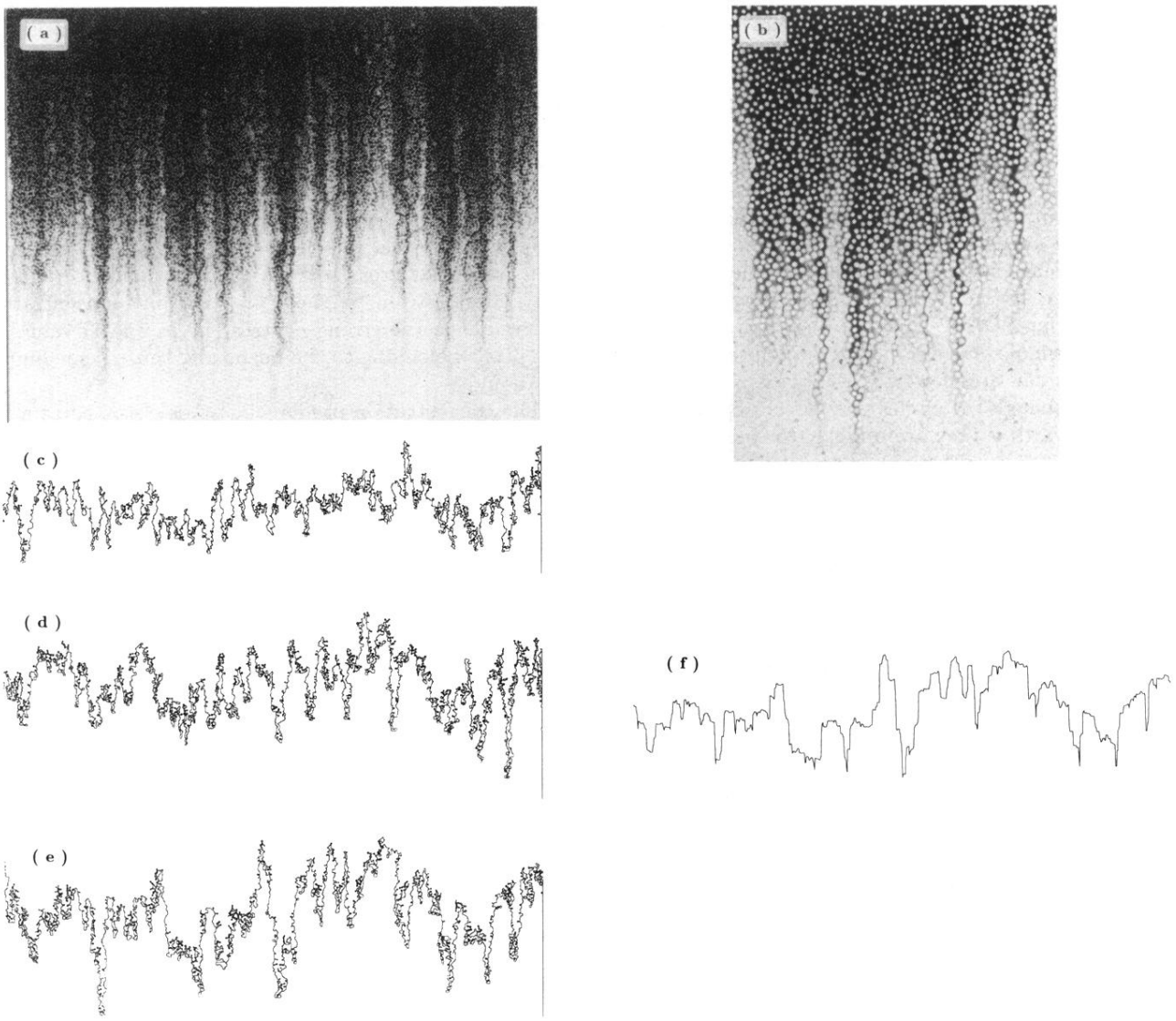

FIG. 2. (a) Digitized photograph of the dispersion front. The experiment was conducted at Péclet number Pe $\simeq 4 \times 10^4$. The size of the image is 1000×700 pixels. (b) Close-up photograph of the dispersion front showing concentration variation from the sub pore size scale up to the tens of pore sizes. White dots in the photo are glass beads. (c)–(e) Development of an equiconcentration dispersion front at relative concentration $C/C_0 = 0.4$. The fronts were taken at times: 135 s (c), 254 s (d), and 400 s (e). The front at time t=400 s was reduced to a single value function by replacing parts of the curve within overhangs by straight line segments in x direction (d).